Electronic structure of puckered group IV-VI two-dimensional monolayer materials

Japanese Journal of Applied Physics

The Japan Society of Applied Physics

REGULAR PAPER • **OPEN ACCESS**

Electronic structure of puckered group IV–VI two-dimensional monolayer materials

OPEN ACCESS

Japanese Journal of Applied Physics **59**, 071006 (2020) **REGULAR PAPER**

https://doi.org/10.35848/1347-4065/ab984c

Electronic structure of puckered group IV–VI two-dimensional monolayer materials

Aflah Zaharo[1*], Acep Purqon[2], Toto Winata[2], and Mineo Saito[3]

[1]*Graduate School of Natural Sciences and Technology, Kanazawa University, Kanazawa 920-1192, Japan*
[2]*Physics Department, Faculty of Mathematics and Natural Science, Institute Technology Bandung, Bandung 40132, Indonesia*
[3]*Faculty of Mathematics and Physics, Institute of Science and Technology, Kanazawa University 920-1192, Japan*

[*]E-mail: aflahzaharo1@gmail.com

Received April 14, 2020; revised May 20, 2020; accepted May 31, 2020; published online June 24, 2020

We carry out first-principle calculations on monolayer group IV–VI 2D materials. We study systems consisting of group IV (C, Si, Ge) and group VI elements (O, S, Se, Te) and find that all the materials form buckled puckered geometries. We clarify that VI atoms tend to be located at the lower positions in the buckled structure when the electronegativity of the VI atom is sufficiently larger than that of the IV atom, which is due to the electron transfer from the IV atom to the VI atom. All the calculated bands are doubly degenerated on the first Brillouin zone edge and this degeneracy can be explained based on the group theory. © 2020 The Japan Society of Applied Physics

1. Introduction

Two-dimensional materials have been stimulating scientific and technological interests because of their novel electronic properties. The discovery of graphene in 2004 opened the gateway into the field of group IV based 2D monolayer materials[1,2] including silicene,[3–6] germanene[7] and stanene.[8] In particular, the Dirac cone in the electronic band structures characterizes the electronic properties of group IV materials.[9]

Phosphorene was successfully synthesized from black phosphorus in 2014.[10–12] In sharp contrast to group IV 2D materials, it was found that phosphorene has a moderate bandgap and is a suitable field-effect transistor material.[13–15] Its bandgap is larger than that of the black phosphorus bulk and decreases as the layer becomes thick, which was first discovered based on a first-principles calculation.[16] As well as phosphorene, other group V materials have been studied such as arsenene,[17–20] antimonene[21–23] and bismuthene.[24–27] The previous calculation showed that the energy difference between the puckered and six-member-ring structures is small[14,28] and they are candidates for optical device and thermoelectric materials.[29]

Recently, IV–VI 2D systems have attracted scientific and technological attention.[28,30,31] The puckered structures are more stable than the six-member-ring one in most of the cases and monolayer systems are candidates for optical device materials.[28,32–36] Therefore, clarification of their electronic structures is necessary.

In this paper, we systematically study the electronic structures of monolayer puckered group IV–VI materials. By performing first-principles density functional based calculations, we first clarify the relation between the buckling amplitudes and the electrons transfer between the IV and VI atoms. Next we analyze the band structures based on the group theory.

2. Method

We first explain our analysis based on the group theory. The symmetry operation $\hat{R}_i$ is given by:

$$\hat{R}_i = \{\hat{\beta}_i|\vec{\tau}_i\}, \tag{1}$$

where $\hat{\beta}_i$ and $\vec{\tau}_i$ represent rotation and fractional translation, respectively.[37] We consider a Bloch wavefunction, $\Psi_k^j(\vec{r})$, given by:

$$\Psi_k^j(\vec{r}) = \frac{1}{\sqrt{NV}} e^{(i\vec{k}\cdot\vec{r})} \sum_n c_j(\vec{G}_n) e^{(i\vec{G}_n\cdot\vec{r})}, \tag{2}$$

where $\vec{G}_n$ and $\vec{k}$ are a reciprocal lattice vector and a wave vector in the first Brillouin zone, respectively. $c_j(\vec{G}_n)$ is a coefficient and the band index j is in the ascending order of energy. N is the total number of unit cells and V is the volume of each unit cell. The irreducible representations of wavefunctions are determined by evaluating the following expression:

$$Q^\alpha = \frac{1}{l} \sum_i \chi^\alpha(\hat{R}_i)^* \langle \Psi | \hat{R}_i | \Psi \rangle, \tag{3}$$

where l and $\chi^\alpha(\hat{R}_i)$ are the order of the group and the character of the irreducible representation of α, respectively, and i runs over the symmetry operations of the k group. When $Q^\alpha = 1 (Q^\alpha = 0)$, the wavefunctions belong to (do not belong to) the αth irreducible representation. By using Eqs. (2), (3) is expressed as:

$$Q^\alpha = \sum_i {}'\chi^\alpha(\hat{R}_i)^* \sum_n c_j(\vec{G}_n)\, c_j(\hat{\beta}_i\vec{G}_n - \vec{G}_i{}')^* \times e^{(-i(\hat{\beta}_i\vec{G}_n - \vec{G}_i{}')\cdot\vec{\tau}_i)}, \tag{4}$$

where $\vec{k}$ satisfies $\hat{\beta}_i\vec{k} = \vec{k} - \vec{G}_i{}'$ for a given reciprocal lattice vector $\vec{G}_i{}'$ ($\vec{G}_i{}' = 0$ when the k point is inside the first Brillouin zone). In the above expression, we introduce the irreducible ray representation whose character is given by:

$${}'\chi^\alpha(\hat{R}_i) = \chi^\alpha(\hat{R}_i) e^{(i\vec{k}\cdot\vec{\tau}_i)}, \tag{5}$$

This irreducible ray representation in most cases corresponds to those of the conventional irreducible representations of the point groups used in the analysis of molecules and thus we use the Mulliken symbols to express the representations.[38,39] However, in some exceptional cases, the irreducible ray representations do not correspond to

conventional irreducible representations as mentioned in the next paragraph. We implemented the above algorithm in the first-principles calculation code PHASE/0.[40)]

In this work, we discuss the degeneracy of the bands based on the group theory. In some cases of non-symmorphic systems, the sticking of bands occurs on the first Brillouin zone edge, i.e., only two-dimensional irreducible ray representations are allowed on the zone boundary and their characters are different from those of the Mulliken ones.

Another type of doubly degeneracy is induced by time-reversal symmetry, which can be checked by calculating the Herring sum.[41)]

$$S = \sum_m \chi^{\alpha}(\hat{Q}_m^2) = \begin{cases} p \text{ (case } a) \\ 0 \text{ (case } b), \end{cases} \quad (6)$$

where $\hat{Q}_m$ is a time-reversal symmetry operation which transforms $\vec{k}$ to $(-\vec{k} + \vec{G}_m)$ for a given reciprocal lattice vector $\vec{G}_m$ and p is the number of time-reversal symmetry operations. In the case of b, two levels belonging to different irreducible representations have the same energy.[41)] On the other hand, this pairing does not occur in the case of a.

To simulate two-dimensional materials, we use slab models; the lattice constant for the c-axis is taken to be so large that the interaction between neighboring slabs along the c-axis is negligible. In the present study, the lattice constant for the c-axis is taken to be 20 Å (Fig. 1). We carry out density functional band structure calculations to obtain the Bloch wavefunctions, $\Psi_k^i(\vec{r})$. We use the exchange-correlation function of the generalized gradient approximation.[42,43)] The ultrasoft[44)] and norm-conserving[45)] pseudopotentials are used for carbon, oxygen, and tellurium and for silicon, sulfur, germanium, and selenium atoms, respectively. We use $15 \times 15 \times 1$ k sampling points in the Brillouin zone integrations.

3. Results and discussion

3.1. Optimized structures and stability monolayers

We first optimize the lattice constants and internal coordinates of the atoms (Table I). We find that the two top atoms are buckled in the optimized structures (Fig. 1) and thus systems belong to the space group $Pmn2_1(C_{2v}^7)$ as well as the group V buckled puckered systems.[28,30,34)] Since this space group is non-symmorphic, some symmetry operations have fractional translations as discussed later. Table I shows the optimized structural parameters, which are close to previous calculational and experimental values.[28,30–36)]

Table I. Calculated structural parameters (a, b, R_1, R_2 and d) which are defined in Fig. 1.

AB	a (Å)	b (Å)	R_1 (Å)	R_2 (Å)	d (Å)
CSe	4.07	3.03	1.96	2.01	1.84
CTe	4.36	4.25	2.16	2.18	2.08
SiO	4.53	2.68	1.83	1.83	1.31
SiS	4.82	3.33	2.26	2.33	2.17
SiSe	4.69	3.67	2.50	2.47	2.38
SiTe	4.36	4.25	2.62	2.76	2.72
GeO	4.45	3.06	1.99	2.00	2.00
GeS	4.67	3.61	2.44	2.44	2.35
GeSe	4.33	3.95	2.55	2.66	2.53
GeTe	4.36	4.25	2.73	2.88	2.72

We define the buckling amplitude (h) which is positive when the group VI atoms are located at the lower positions (Fig. 1). We find that as the difference in the electronegativity $\xi_B - \xi_A$ becomes large, h tends to increase (Fig. 2 and Table II), where ξ_A and ξ_B are the electronegativities of the group IV and VI atoms, respectively. When $\xi_B - \xi_A$ is sufficiently large (SiO, SiS, SiSe, GeO and GeS), i.e., $\xi_B - \xi_A > 0.54$, the VI atoms are located at the lower positions and thus h is positive. In contrast, when $\xi_B - \xi_A$ is negative (CTe), the VI atoms are located at the higher positions and h is negative. We also find that h is negative when $\xi_B - \xi_A$ is positively small (CSe, SiTe, GeSe and GeTe), i.e., $0 < \xi_B - \xi_A < 0.54$.

Here we discuss the reason why the group VI atoms are located at the lower positions when $\xi_B - \xi_A$ is large. Electrons substantially transfer from the IV atom to VI atom when $\xi_B - \xi_A$ is large. In this case, the VI atoms are expected to be located at the lower positions because as

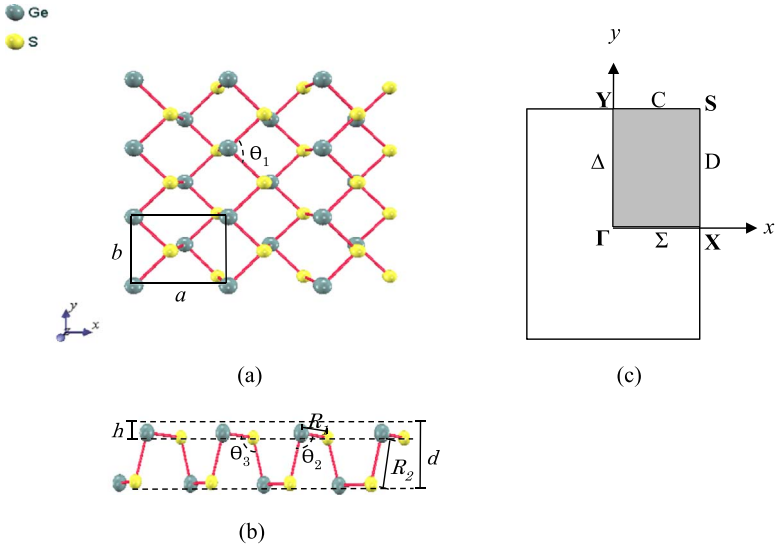

Fig. 1. (Color online) Top (a) and side (b) views of the buckled puckered structure and the first Brillouin zone (c). Blue and yellow balls represent group IV and group VI atoms, respectively.

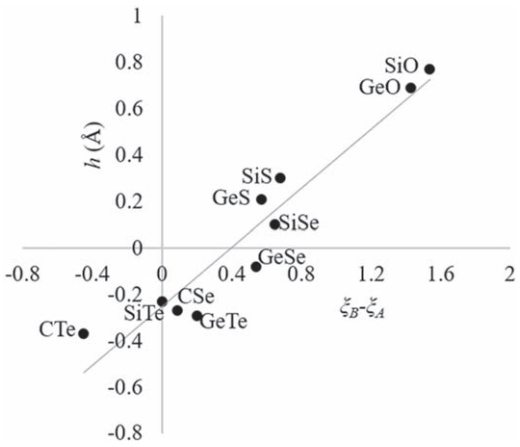

Fig. 2. (Color online) Relationship between the buckling height, h, and the difference of electronegativities, $\xi_B - \xi_A$.

Table II. Geometrical parameters and the difference of the electronegativities, $\xi_B - \xi_A$, which are determined by the Pauling scale.[30] The buckling amplitude, h, and the bond angles, θ_2 and θ_3, are defined in Fig. 1.

	θ_2	θ_3	$\theta_3 - \theta_2$	h	$\xi_B - \xi_A$
CSe	110.9	98.2	−12.7	−0.23	0.00
CTe	109.3	90.1	−19.2	−0.37	−0.45
SiO	94.2	132.5	38.3	0.77	1.54
SiS	96.3	111.1	14.8	0.3	0.68
SiSe	97.0	101.5	4.5	0.1	0.65
SiTe	100.3	87.8	−12.5	−0.29	0.20
GeO	91.3	126.5	35.2	0.69	1.43
GeS	94.9	106.2	11.3	0.21	0.57
GeSe	96.8	92.4	−4.4	−0.08	0.54
GeTe	99.9	87.3	−12.6	−0.27	0.09

Table II shows, the lower position atoms have larger bond angles and thus their orbitals are energetically stabilized as a consequence of large s component. As discussed in a previous paper,[14,16] this electron transfer from the higher position atom to the lower position atom also occurs even when the two atoms are of the same kind; this type of electron transfer occurs in the case of the buckled puckered structure of group V two-dimensional systems.[14]

To check the validity of the above argument, we take GeS as an example and calculate the electron density for the valence band top (VBT) and conduction band bottom (CBB) (Fig. 3). The electronegativity of S is sufficiently larger than that of Ge ($\xi_B - \xi_A = 0.57$) and the Ge and S atoms are located at the higher and the lower positions, respectively. As Fig. 3 shows, VBT and CBB mainly consist of S and Ge orbitals, respectively, which indicates that electrons transfer from Ge to S. Since the bond angle of S is larger than that of Ge, the orbitals of S include large s components, which stabilizes the orbitals (Fig. 3).

3.2. Band structures of the monolayer analyzed based on the group theory

We calculate the band structures of the monolayer systems. In most parts of the Brillouin zone, wavefunctions belong to conventional irreducible representations. In this case, we use Mulliken symbols in Fig. 4.[38,39] In the other cases, we use the numerical notations.

We clarify that all the bands are doubly degenerated on the zone edge (Fig. 4). First, we discuss the degeneracy on the S–C–Y line where the k group has the symmetry of C_{2v}

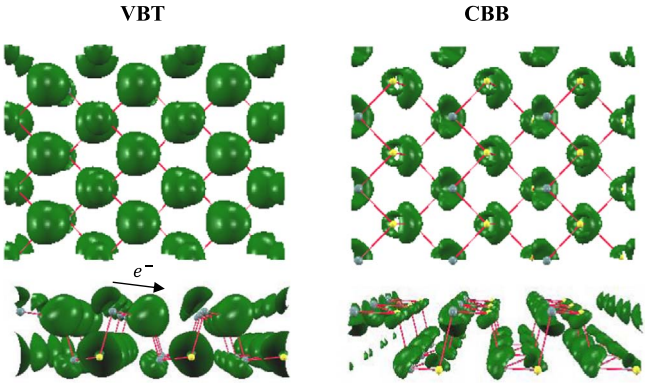

Fig. 3. (Color online) Electron density for the VBT (left-hand side) and CBB (right-hand side) of GeS. We integrate the electron densities over the energy width of 0.2 eV to the VBT (a) and from the CBB (b).

(Table IV) and symmetry operations $\{C_2(x)|\vec{\tau}\}$ and $\{\sigma_{xy}|\vec{\tau}\}$ include the fractional translation $\vec{\tau} = \frac{1}{2}\vec{a} + \frac{1}{2}\vec{b}$, where $\vec{a}$ and $\vec{b}$ are primitive lattice vectors in the x and y directions, respectively. When $e^{\{i(\hat{\beta}_i - \vec{k})\cdot\vec{\tau}_i\}} \neq 1$ for an operation $\{\hat{\beta}_i|\vec{\tau}_i\}$, the wavefunctions do not belong to the conventional irreducible representation.[46] We find that $D = e^{\{i(C_2(x) - \vec{k})\cdot\vec{\tau}\}} = -1$ (Table IV) and therefore the wavefunctions do not belong to conventional irreducible representations; only one irreducible ray representation Γ_1 whose characters are shown in Table III is allowed. Since Γ_1 is two-dimensional, the sticking of bands occurs on the S–C–Y line, i.e., all the bands are doubly degenerated.

On the other hand, on the X–D line, the wavefunctions belong to conventional irreducible representations denoted by Mulliken symbols because of $D = 1$. We find that all the bands belong to a one-dimensional representation since the symmetry is not high (C_{2v} and C_s) as Fig. 4 shows. However, we find that all the bands are paired because of the time-reversal symmetry.[47] We evaluate the Herring sum in Eq. (6) and find that the sum equals to 0, indicating that two different irreducible representations are paired (Table IV). As Table IV shows, A_1 and B_1 (A_2 and B_2) are paired at the X point where the symmetry is C_{2v}. A' and A'' are paired on the D line where the symmetry is C_s.

Based on the argument mentioned above, we conclude that the degeneracy on the first Brillouin zone edge is due to the symmetry of this system. The degeneracy on the S–C–Y line occurs due to the sticking of the bands on the first Brillouin zone edge. Meanwhile, for the X–D line, the degeneracy is caused by the time-reversal symmetry. The above-mentioned degeneracy on the Brillouin zone edge is expected to be detected by some experiments such as photoelectron spectroscopy. This degenerated bands may split when we include the spin-orbit coupling.[48]

4. Conclusion

We have carried out first-principles calculations of group IV–VI two-dimensional monolayer materials. The systems form buckled geometries and thus the space group is $Pmn2_1(C_{2v}^7)$. We conclude that when the electronegativity difference ($\xi_B - \xi_A$) is large, the group VI atoms are located at the lower positions. This is because electrons transfer from the higher position atom to the lower position atom. On the contrary, if the difference is positively small or negative,

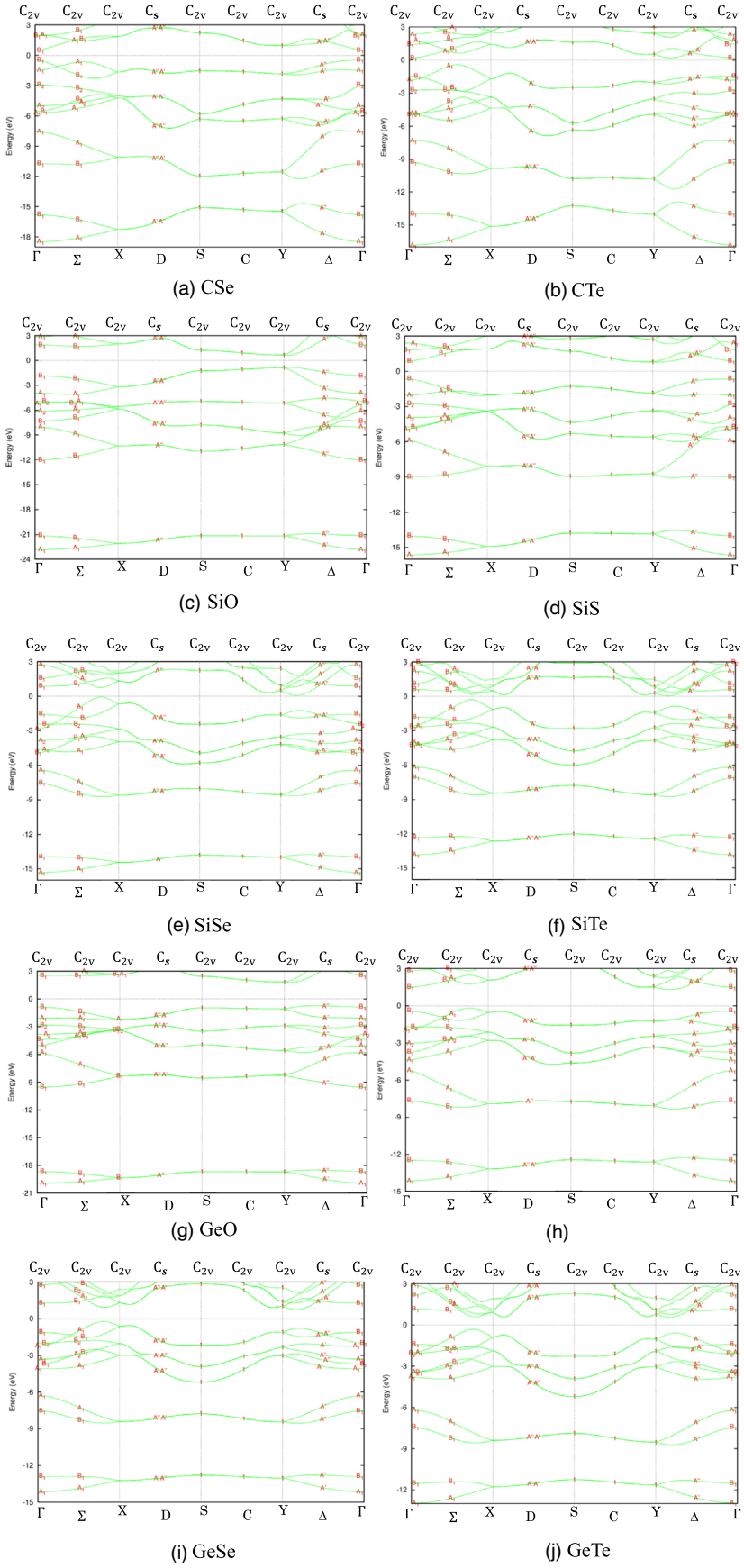

Fig. 4. (Color online) Band structures of buckled puckered structures of (a) CSe (b) CTe (c) SiO (d) SiS (e) SiSe (f) SiTe (g) GeO (h) GeS (i) GeSe (j) GeTe. We use Mulliken symbols for one-dimensional irreducible representations (A_1,A_2,B_1,B_2) for Γ, Σ, X line and A', A'' for the D line. We denote Γ_1 by 1 on the S–C–Y line in the figures.

Table III. Character table for k groups.

	Irreducible Representation	E	$C_2(x)$	σ_{xz}	σ_{xy}
$X(C_{2v})$	A_1	1	−1	−1	−1
	A_2	1	−1	−1	−1
	B_1	1	−1	−1	−1
	B_2	1	−1	−1	−1
$S(C_{2v})$	Γ_1	2	0	0	0
$C(C_{2v})$	Γ_1	2	0	0	0
$Y(C_{2v})$	Γ_1	2	0	0	0
$D(C_s)$	A'	1			−1
	A''	1			−1

Table IV. Group theoretical analysis for some k points.

k point	Point group	Symmetry operation	D	Irreducible representation	Time-reversal element	Herring sum	Pairing
Γ	C_{2v}	$\{E\|0\}$ $\{C_2(x)\|\vec{\tau}\}$ $\{\sigma_{xz}\|0\}$ $\{\sigma_{xy}\|\vec{\tau}\}$	1	A_1, B_1, A_2, B_2	$\{E\|0\}$ $\{C_2(x)\|\vec{\tau}\}$ $\{\sigma_{xz}\|0\}$ $\{\sigma_{xy}\|\vec{\tau}\}$	4	No pairing
Σ	C_{2v}	$\{E\|0\}$ $\{C_2(x)\|\vec{\tau}\}$ $\{\sigma_{xz}\|0\}$ $\{\sigma_{xy}\|\vec{\tau}\}$	1	A_1, B_1, A_2, B_2	No time-reversal element	—	No pairing
X	C_{2v}	$\{E\|0\}$ $\{C_2(x)\|\vec{\tau}\}$ $\{\sigma_{xz}\|0\}$ $\{\sigma_{xy}\|\vec{\tau}\}$	1	A_1, B_1, A_2, B_2	$\{E\|0\}$ $\{C_2(x)\|\vec{\tau}\}$ $\{\sigma_{xz}\|0\}$ $\{\sigma_{xy}\|\vec{\tau}\}$	0	(A_1, B_1) (A_2, B_2)
D	C_s	$\{C_2(x)\|\vec{\tau}\}$ $\{\sigma_{xy}\|\vec{\tau}\}$	1	A', A''	$\{C_2(x)\|\vec{\tau}\}$ $\{\sigma_{xy}\|\vec{\tau}\}$	0	(A', A'')
S	C_{2v}	$\{E\|0\}$ $\{C_2(x)\|\vec{\tau}\}$ $\{\sigma_{xz}\|0\}$ $\{\sigma_{xy}\|\vec{\tau}\}$	−1	Γ_1	$\{E\|0\}$ $\{C_2(x)\|\vec{\tau}\}$ $\{\sigma_{xz}\|0\}$ $\{\sigma_{xy}\|\vec{\tau}\}$	4	No pairing
C	C_{2v}	$\{E\|0\}$ $\{C_2(x)\|\vec{\tau}\}$ $\{\sigma_{xz}\|0\}$ $\{\sigma_{xy}\|\vec{\tau}\}$	−1	Γ_1	No time-reversal element	—	No pairing
Y	C_{2v}	$\{E\|0\}$ $\{C_2(x)\|\vec{\tau}\}$ $\{\sigma_{xz}\|0\}$ $\{\sigma_{xy}\|\vec{\tau}\}$	−1	Γ_1	$\{E\|0\}$ $\{C_2(x)\|\vec{\tau}\}$ $\{\sigma_{xz}\|0\}$ $\{\sigma_{xy}\|\vec{\tau}\}$	4	No pairing
Δ	C_s	$\{C_2(x)\|\vec{\tau}\}$ $\{\sigma_{xy}\|\vec{\tau}\}$	1	A', A''	$\{C_2(x)\|\vec{\tau}\}$ $\{\sigma_{xy}\|\vec{\tau}\}$	2	No pairing

group VI atom is located at the higher positions. We find that all the bands are doubly degenerated on the first Brillouin zone edge and clarify that this degeneracy is explained based on the group theory.

Acknowledgments

This work was partly supported by Grants-in-Aid for Scientific Research (No. 17K05118) from the Japan Society for the Promotion of Science (JSPS). The computations in this research were performed using the supercomputers at the Institute for Solid State Physics (ISSP) at the University of Tokyo. The authors (A. Z.) acknowledges financial support from the Japanese Government (KU) Scholarship Program.

1) K. S. Novoselov, A. K. Geim, S. V. Morozov, D. Jiang, Y. Zhang, S. V. Dubonos, I. V. Grigorieva, and A. A. Firsov, Science **306**, 666 (2004).
2) G. Eda, G. Fanchini, and M. Chhowalla, Nat. Nanotech. **3**, 270 (2008).
3) S. Cahangirov, M. Topsakal, E. Aktürk, H. Sahin, and S. Ciraci, Phys. Rev. Lett. **102**, 236804 (2009).
4) P. Vogt, P. D. Padova, S. Quaresima, J. Avila, E. Frantzeskakis, M. C. Asensio, A. Resta, B. Ealet, and G. L. Lay, Phys. Rev. Lett. **108**, 155501 (2012).
5) S. Huang, W. Kang, and L. Yang, Appl. Phys. Lett. **102**, 133106 (2013).
6) K. Takeda and K. Shiraishi, Phys. Rev. B **50**, 14916 (1994).
7) E. Bianco, S. Butler, S. Jiang, O. D. Restrepo, W. Windi, and J. E. Goldberger, ACS Nano. **7**, 4414 (2013).
8) F. F. Zhu, W. J. Chen, Y. Xu, C. L. Gao, D. D. Guan, D. Qian, S. C. Zhang, and J. F. Jia, Nat. Mater. **14**, 1020 (2015).
9) B. Liu and K. Zhou, Prog. Mater. Sci. **100**, 99 (2019).
10) L. Li, Y. Yu, G. J. Ye, Q. Ge, X. Ou, H. Wu, D. Feng, X. H. Chen, and Y. Zhang, Nat. Nanotech. **9**, 372 (2014).
11) H. Liu, A. T. Neal, Z. Zhu, Z. Luo, X. Xu, D. Tomanek, and P. D. Ye, ACS Nano. **8**, 4033 (2014).
12) E. S. Reich, Nature **506**, 19 (2014).
13) T. Hong, B. Chamlagain, W. Lin, H. J. Chuang, M. Pan, Z. Zhou, and Y. Q. Xu, Nanoscale. **6**, 8978 (2014).
14) A. P. N. Nuning and M. Saito, Jpn. J. Appl. Phys. **58**, 061003 (2019).
15) J. S. Qiao, X. H. Kong, Z. Hu, F. Yang, and W. Ji, Nat. Commun. **5**, 4475 (2014).

16) M. Saito, Y. Takemori, T. Hashi, T. Nagao, and S. Yaginuma, Jpn. J. Appl. Phys. **46**, 7824 (2007).
17) C. Kamal and M. Ezawa, Phys. Rev. B **91**, 085423 (2015).
18) Y. Xu, B. Peng, H. Zhang, H. Shao, R. Zhang, and H. Zhu, Ann. Phys. (Berlin) **529**, 1600152 (2017).
19) M. Pumera and Z. Sofer, Adv. Mater. **29**, 1605299 (2017).
20) S. Sharma, S. Kumar, and U. Schwingenschlögl, Phys. Rev. Appl. **8**, 044013 (2017).
21) O. U. Aktürk, V. O. Ozcelik, and S. Ciraci, Phys. Rev. B **91**, 235446 (2015).
22) M. F. Deschênes, O. Waller, T. O. Menteş, A. Locatelli, S. Mukherjee, F. Genuzio, P. L. Levesque, A. Hébert, R. Martel, and O. Moutanabbir, Nano Lett. **17**, 4970 (2017).
23) P. Ares, J. J. Palacios, G. Abellán, J. G. Herrero, and F. Zamora, Adv. Mater. **30**, 1703771 (2017).
24) E. Aktürk, O. U. Aktürk, and S. Ciraci, Phys. Rev. B **94**, 014115 (2016).
25) M. Y. Liu, Y. Huang, Q. Y. Chen, Z. Y. Li, C. Cao, and Y. He, RSC Adv. **7**, 39546 (2017).
26) T. Nagao, J. T. Sadowski, M. Saito, S. Yaginuma, Y. Fujikawa, T. Kogure, T. Ohno, Y. Hasegawa, S. Hasegawa, and T. Sakurai, Phys. Rev. Lett. **93**, 105501 (2004).
27) M. Saito, T. Ohno, and T. Miyazaki, Appl. Surf. Sci. **237**, 80 (2004).
28) Z. Hu, Y. Ding, X. Hu, W. Zhou, X. Yu, and S. Zhang, Nanotech. **30**, 252001 (2019).
29) Y. Tanaka, M. Saito, and F. Ishii, Jpn. J. Appl. Phys. **57**, 125201 (2018).
30) C. Kamal, A. Chakrabarti, and M. Ezawa, Phys. Rev. B **91**, 125428 (2016).
31) R. Fei, W. Li, J. Li, and L. Yang, Appl. Phys. Lett. **107**, 173104 (2015).
32) B. R. Tuttle, S. M. Alhassan, and S. T. Pantelides, Phys. Rev. **92**, 235405 (2016).
33) F. Li, X. H. Liu, Y. Wang, and Y. F. Li, J. Mater. Chem. C. **4**, 2155 (2016).
34) T. Hu and J. Dong, Phys. Chem. Chem. Phys. **18**, 32514 (2016).
35) S. L. Zhang, N. Wang, S. G. Liu, S. P. Huang, W. H. Zhou, B. Cai, M. Q. Xie, Q. Yang, X. P. Chen, and H. B. Zeng, Nanotech. **27**, 274001 (2016).
36) Z. Ma, B. Wang, L. Ou, Y. Zhang, X. Zhang, and Z. Zhou, Nanotech. **27**, 415203 (2016).
37) V. Heine, *Group Theory in Quantum Mechanics* (Pergamon, London, 1960).
38) R. S. Mulliken, J. Chem. Phys. **23**, 1997 (1955).
39) R. S. Mulliken, J. Chem. Phys. **24**, 1118 (1956).
40) PHASE/0 [https://azuma.nims.go.jp/cms1].
41) M. S. Dresselhaus, G. Dresselhaus, and A. Jario, *Group Theory* (Springer, Berlin, 2008).
42) J. P. Perdew and Y. Wang, Phys. Rev. B **45**, 13244 (1992).
43) J. P. Perdew, K. Burke, and M. Ernzerhof, Phys. Rev. Lett. **77**, 3865 (1996).
44) D. Vanderbilt, Phys. Rev. B **41**, 7892 (1990).
45) D. R. Hamann, M. Schlüter, and C. Chiang, Phys. Rev. Lett. **43**, 1494 (1979).
46) L. Bolin, *Nonsymmorphic Symmetries and Their Consequences* (Massachusetts Institute of Technology, Cambridge, MA, 2012).
47) G. Burns, in *Introduction to Group Theory with Applications*, ed. A. M. Alper and A. S. Nowick (Academic, New York, 1977), p. 323.
48) S. D. Guo and Y. H. Wang, J. Appl. Phys. **121**, 034302 (2017).